Appl. Phys. A 80, 1197–1209 (2005)
DOI: 10.1007/s00339-004-3172-2

Applied Physics A
Materials Science & Processing

P.M. MENDES
A.H. FLOOD
J.F. STODDART✉

Nanoelectronic devices from self-organized molecular switches

California NanoSystems Institute and Department of Chemistry and Biochemistry, University of California, Los Angeles, 405 Hilgard Avenue, Los Angeles, CA 90095-1569, USA

Received: 12 October 2004 / Accepted: 23 November 2004
Published online: 11 March 2005 •

ABSTRACT The development of molecular electronic switching devices for memory and computing applications presents one of the most exciting contemporary challenges in nanoscience and nanotechnology. One basis for such a device is a two-terminal molecular-switch tunnel junction that can be electrically switched between high- and low-conductance states. Towards this end, the concepts of self-assembly and molecular recognition have been pursued actively for synthesizing two families of redox-controllable mechanically interlocked molecules – bistable catenanes and bistable rotaxanes – as potential candidates for solid-state molecular-switch tunnel junctions. This article reviews logically the development and understanding of Langmuir, Langmuir–Blodgett and self-assembled monolayers of amphiphilic bistable and functionalized bistable rotaxanes and their catenanes counterparts. Our increased understanding of the superstructures of these monolayers has guided our recent efforts to incorporate these self-organized molecular switches into devices. The methodologies that are being employed are in their early stages of development. Certain characteristics of the molecules, monolayers, electrodes and devices are emerging that serve as lessons to be consider in responding to the ample opportunities for further research and process development in the field of nanoelectronics.

PACS 81.07.-b; 81.07.Nb; 85.65.+h

1 Introduction

The manufacture of nanometer-scale electronic devices in a time and cost effective manner remains a challenging task. While the traditional semiconductor fabrication approach is based on lithographic "top-down" techniques [1], the construction of nanodevices utilizing the assembly of molecular-sized components – the so-called "bottom-up" chemical approach – offers a number of very attractive advantages [2]. As feature sizes in electronic circuits, based on complementary metal-oxide semiconductors (CMOS) move into the nanometer-size regime, fundamental physical limitations in using top-down approaches begin to emerge and are reflected in the transition from classical to quantum physics [3]. For example, size quantization opens up significant gaps between energy levels and influences the rates of electron tunneling through ultra-thin insulating barriers. On the other hand, bottom-up approaches using molecules as active components (e.g., switches [4, 5], sensors [6], light emitting diodes [7]) or passive components (e.g., rectifiers [8]) of electronic circuits, promise experimental and manufacturing simplicity down to the atomic size scale, lower power consumption and the potential for low-cost mass fabrication [9]. Molecular electronics research is advancing at a fast pace, with commercial applications (e.g., ZettaCore [10]) just starting to emerge.

In the context of switchable molecules in electronic devices [11, 12], molecular recognition phenomena that are amenable to being altered by redox activation/deactivation are particularly appealing. With this proviso in mind, we have designed and synthesized, using template-directed protocols [13], a considerable number of bistable molecular and supramolecular systems. These systems are generally composed of π-electron rich and poor components held together by noncovalent bonds and, more often than not, also by mechanical bonds – i.e., they are interlocked molecules [14] in the form of either bistable catenanes (Scheme 1) or bistable rotaxanes (Scheme 2).

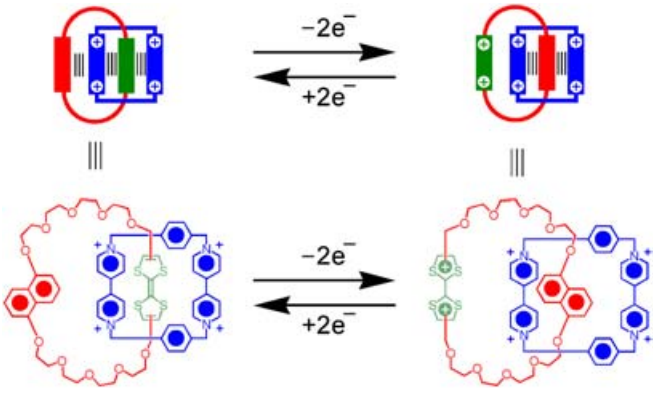

Scheme 1. Graphical representation and structural formula of a bistable [2]catenane, illustrating the solution-phase redox-controllable switching mechanism

✉ Fax: +1-310-206-1843, E-mail: stoddart@chem.ucla.edu

Switchable catenanes and rotaxanes have been developed in our research laboratories apace by focusing upon their optimization and customization. One of the most efficient of these catenanes [15] is composed of a tetracationic macrocycle, cyclobis(paraquat-*p*-phenylene) ($CBPQT^{4+}$), that is interlocked (Scheme 1) with a macrocyclic polyether incorporating a tetrathiafulvalene (TTF) unit and a dioxynaphthalene (DNP) ring system. In solution, the TTF unit resides preferentially inside the cavity of the tetracationic macrocycle of the [2]catenane. Upon oxidation, however, the neutral TTF unit is converted into either its monocationic ($TTF^{+\bullet}$) or dicationic (TTF^{2+}) form. These positively charged units are expelled from the cavity of the tetracationic macrocycle and replaced by a neutral DNP ring system, following circumrotation (Scheme 1) of the macrocyclic polyether through the cavity of the tetracationic macrocycle. Upon reduction, neutrality is restored to the TTF unit and another circumrotation regenerates the original state.

In their simplest manifestation, rotaxanes are composed of mutually recognizable and intercommunicating macrocycle and dumbbell-shaped components. One of the best examples (Scheme 2) of a bistable, redox-switchable rotaxane consists [16] of a tetracationic macrocycle component and a linear rod section that contains two different stations – a TTF unit and a DNP ring system – separated by a spacer group

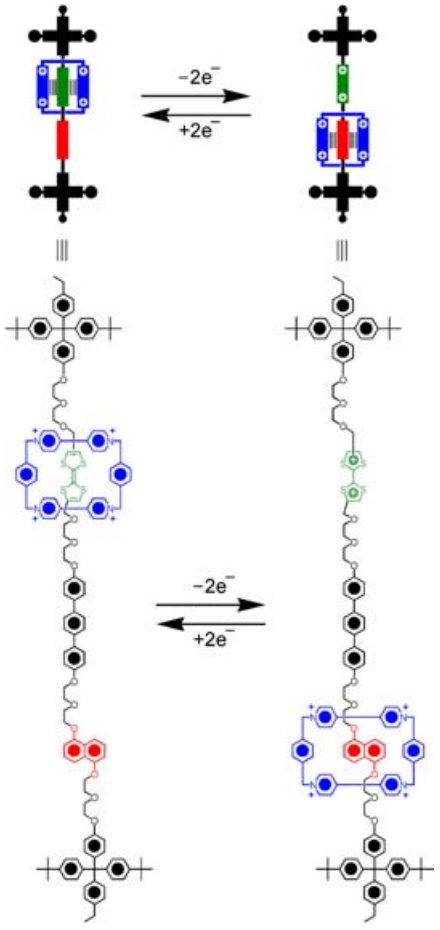

Scheme 2. Graphical representation and structural formula of a bistable [2]rotaxane, illustrating the solution-phase redox-controllable switching mechanism

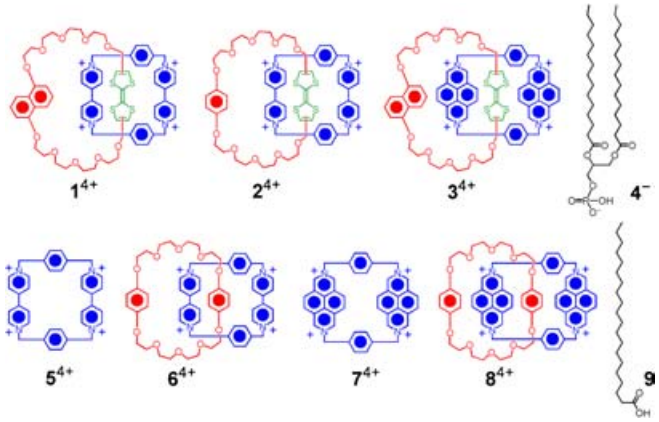

Scheme 3. Structural formulas of switchable catenanes ($\mathbf{1}^{4+}$, $\mathbf{2}^{4+}$, $\mathbf{3}^{4+}$) together with the hydrophilic dimyristoylphosphatidyl counteranion ($\mathbf{4}^{-}$, $DMPA^{-}$) and their respective control molecules ($\mathbf{5}^{4+}$, $\mathbf{6}^{4+}$, $\mathbf{7}^{4+}$, $\mathbf{8}^{4+}$, **9**), which were used in the fabrication and testing of molecular-based electronic devices

and terminated by two bulky tetraarylmethane stoppers. The switching mechanism proceeds in a very similar manner to that observed for bistable catenanes. The starting state of the bistable rotaxane (Scheme 2) has its TTF unit encircled by the tetracationic macrocycle. Upon oxidation, the TTF unit becomes mono- or dicationic, causing the macrocycle to shuttle (Scheme 2) toward the DNP ring system in the oxidized state. Conversely, reduction of the TTF^{2+} dication back to a neutral TTF unit causes the rotaxane to return to its starting state. Thus, this bistable rotaxane, with these two reversibly switchable redox states involving macrocycle translation, has been referred to as a molecular shuttle [17].

The magnitudes of the noncovalent bonding interactions that control the locations of the macrocycles in bistable catenanes and rotaxanes can be switched reversibly in solution by redox processes triggered by chemical [15, 18–20], electrochemical [19–22], and/or photochemical stimuli [22–24]. Such controllable molecular switches have been demonstrated [12, 18, 22–24] to operate successfully in solution by ^{1}H NMR spectroscopy, UV/Vis spectroscopy and cyclic voltammetry. This type of molecular actuation, which can be optimized rationally through molecular design and synthesis, provides the basis for information storage by defining the "open" and "closed" states of a switch.

Nevertheless, molecular synthesis is a solution-phase endeavor, and if these bistable molecular compounds are to find applications in nanoelectronic devices, it is essential that these entities become organized within solid-state devices. Moreover, the same level of control over dynamic motion in bistable molecular compounds that has been established in the solution state needs to be maintained in the devices. The methodology, by which we have chosen [25–32] to pursue this goal of transferring controllable molecular switches from the solution phase into solid-state devices, is self-organization, using either the Langmuir–Blodgett (LB) technique or self-assembled monolayers (SAMs).

In this review, we will highlight some of the recent advances that have been made toward the self-organization of a range (Schemes 3 and 4) of molecular and supramolecu-

lar entities, as well as the superstructures of the molecules within the monolayers as an introduction to how they operate in molecular-switch tunnel junction (MSTJ) devices. The binary switching character, obtained from a range of devices incorporating a variety of bistable molecular switches, will be presented alongside the control devices constructed around non-switchable molecules. Finally, the key ingredients for the design of new classes of devices and molecules will be reviewed in the light of research that has been accomplished to date.

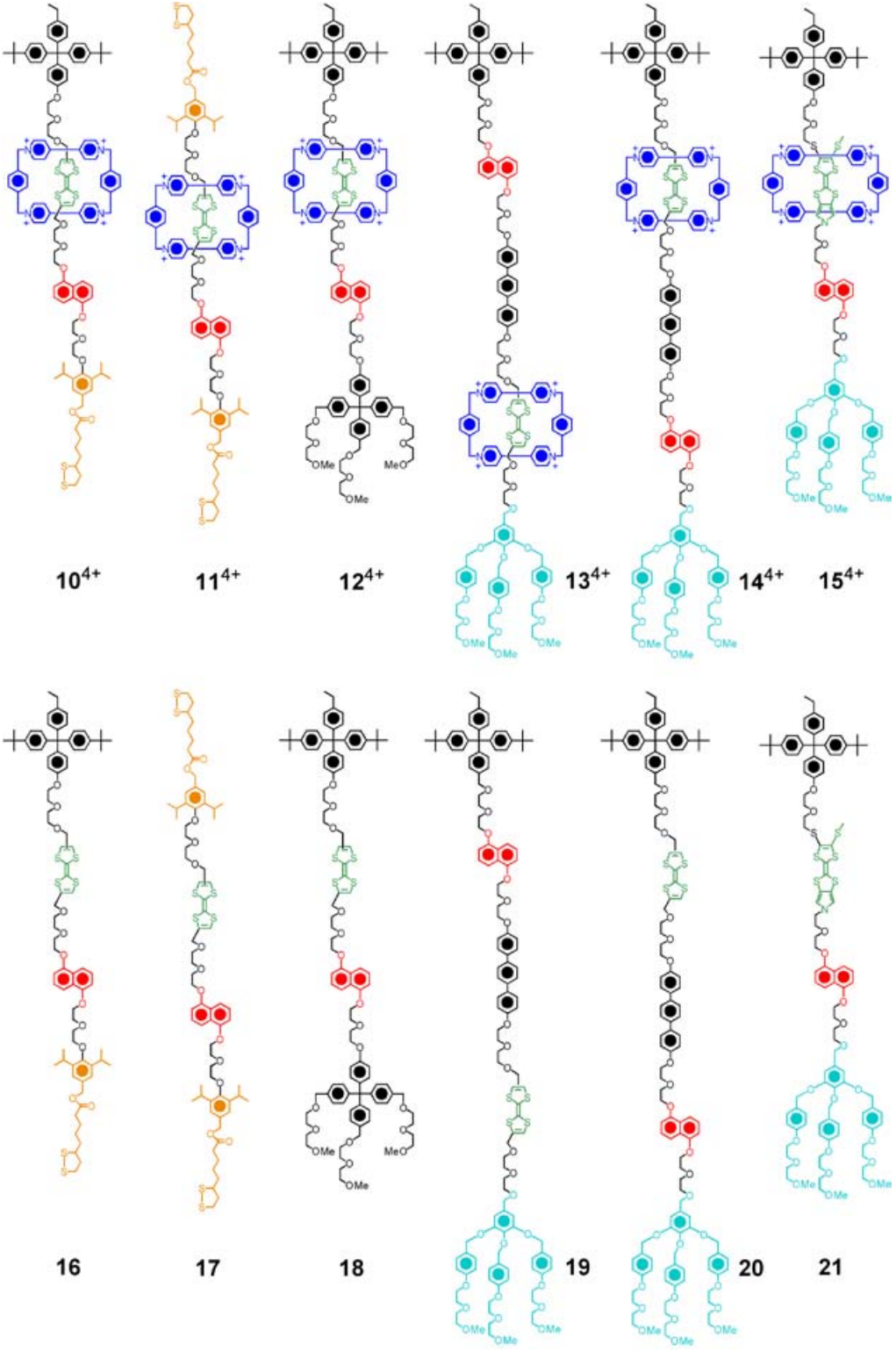

Scheme 4. Structural formulas of switchable rotaxanes ($\mathbf{10}^{4+}$, $\mathbf{11}^{4+}$, $\mathbf{12}^{4+}$, $\mathbf{13}^{4+}$, $\mathbf{14}^{4+}$, $\mathbf{15}^{4+}$), together with their respective dumbbell control molecules (**16**, **17**, **18**, **19**, **20**, **21**), which were used in the fabrication and testing of molecular-based electronic devices

2 Catenanes in monolayers and in devices

The mechanical switching properties of bistable catenanes have been investigated with the aim [5, 33, 34] of constructing molecular electronic devices. Since the incorporation of catenanes into thin films is required for the preparation of such devices, the past several years has witnessed a considerable growth in the study of bistable catenanes – namely, $\mathbf{1}^{4+}$, $\mathbf{2}^{4+}$ and $\mathbf{3}^{4+}$ (Scheme 3) – that can be self-organized [25–29] at the air-water interface with the aid of the amphiphilic dimyristoylphosphatidyl counteranion $\mathbf{4}^{-}$ ($DMPA^{-}$). Monostable compounds are essential for use in control experiments. They have included (i) the tetracationic macrocycle $\mathbf{5}^{4+}$ present in the bistable catenanes $\mathbf{1}^{4+}$ and $\mathbf{2}^{4+}$, (ii) the monostable degenerate [2]catenane $\mathbf{6}^{4+}$, wherein the same tetracationic macrocycle is interlocked with bis-*p*-phenylene-34-crown-10 (BPP34C10), as well as (iii) the tetracationic macrocycle $\mathbf{7}^{4+}$ present in the bistable catenane $\mathbf{3}^{4+}$, (iv) the monostable degenerate [2]catenane $\mathbf{8}^{4+}$, wherein the same tetracationic macrocycle is interlocked with BPP34C10, and, in addition, (v) the non-redox active eicosanoic acid **9**.

An organic thin film can be deposited onto a solid substrate using various techniques, e.g., by spin-coating [35], by atmospheric-pressure ion deposition thermal evaporation [36], by applying the Langmuir–Blodgett (LB) procedure [37, 38] and by self-assembly [38–40]. One possible approach towards structurally ordered bistable catenane assemblies is the preparation of Langmuir films at the air-water interface and their subsequent transfer onto solid substrates by the LB technique. However, bistable catenanes, incorporating the tetracationic ($CBPQT^{4+}$) macrocycle, are characterized by possessing only polar properties, a feature which renders them unable to self-organize in a stable manner at an air-water interface. This limitation has been overcome by associating the catenanes with an amphiphilic compound to produce mixed Langmuir films. For instance, in our research, we have been employing [25–29] the electrostatic interactions between the head groups of the anion $DMPA^{-}$ and the catenane tetracations to form Langmuir films and subsequently LB monolayers.

Prior to carrying out a detailed investigation of LB film deposition of any given molecule, it is necessary to understand the equilibrium and dynamic properties of Langmuir films composed of the same molecules. As a first step, the ability for the tetracationic macrocycle $\mathbf{5}^{4+}$ to form Langmuir monolayers with $DMPA^{-}$ counterions at the air-water interface was investigated [26]. UV/visible spectroscopy and surface pressure versus mean molecular area (π-A) isotherm studies suggested that four $DMPA^{-}$ anions are associated with one tetracationic macrocycle, and that, at a surface pressure corresponding to 1.7 nm^2/molecule, the mean plane of the tetracationic macrocycle is parallel to the air-water interface. This superstructure leads to favorable packing of $DMPA^{-}$ anions, producing well organized monolayers.

Having established that the tetracationic macrocycles form well-organized and stable Langmuir films, more complex entities – namely, pseudorotaxanes [25] and the degenerate [2]catenane $\mathbf{6}^{4+}$ [27] – were self-organized at the air-water interface. Catenanes $\mathbf{1}^{4+}$ and $\mathbf{2}^{4+}$ that possess molecular switching properties, have also been employed [28] – together with $DMPA^{-}$ ($\mathbf{4}^{-}$) counterions – to generate stable Langmuir monolayers. π-A Isotherms have revealed that the organization of the cationic and anionic components was consistent with previous investigations [26] on the bipyridinium-based tetracationic macrocycle $\mathbf{5}^{4+}/4\cdot\mathbf{4}^{-}$. The Langmuir monolayer of [2]catenane $\mathbf{1}^{4+}/4\cdot\mathbf{4}^{-}$ is believed to be stabilized by [π–π] stacking interactions between adjacent catenane molecules, which occur in an alternating manner, allowing each π-donor unit to be positioned side-by-side with a π-acceptor unit and vice-versa. Moreover, the mean molecular area of the catenanes $\mathbf{1}^{4+}$ and $\mathbf{2}^{4+}$ were 1.2 and 1.1 nm^2/molecule, which suggests that the catenanes are aligned (Fig. 1a), such that the mean plane of the tetracationic macrocycle is lying approximately parallel to the air-water interface while the mean plane of the macrocyclic polyether component is roughly perpendicular to the interface. The $DMPA^{-}$ anions are believed to be stacked in a tight and fully-occupied layer above that of the tetracationic catenane. On the other hand, in their chemically-oxidized hexacationic states, the [2]catenanes $\mathbf{1}^{6+}$ and $\mathbf{2}^{6+}$ occupy 1.5 and 1.2 nm^2/molecule and are believed to be lying on the surface of the water in a manner similar to those of $\mathbf{1}^{4+}$ and $\mathbf{2}^{4+}$ with the six $DMPA^{-}$ anions residing more or less on top of the hexacationic [2]catenanes. The catenanes were pre-oxidized with three equivalents of $Fe(ClO_4)_3$ in the spreading co-solvent, i.e., Me_2CO : MeOH (13 : 7).

The stable Langmuir films obtained from the catenanes can be transferred successfully as LB films onto solid substrates – e.g., hydrophobized quartz [27], mica [28], gold [28], silicon [5, 33] and carbon nanotubes [34]. The quality of an LB monolayer deposition is dependent [37, 38] on a variety of processing conditions, such as temperature, compression rate, and subphase salt concentration. For instance, we have demonstrated [28] that the [2]catenanes $\mathbf{1}^{4+}$ and $\mathbf{2}^{4+}$ (Scheme 3), which we know can be switched between dif-

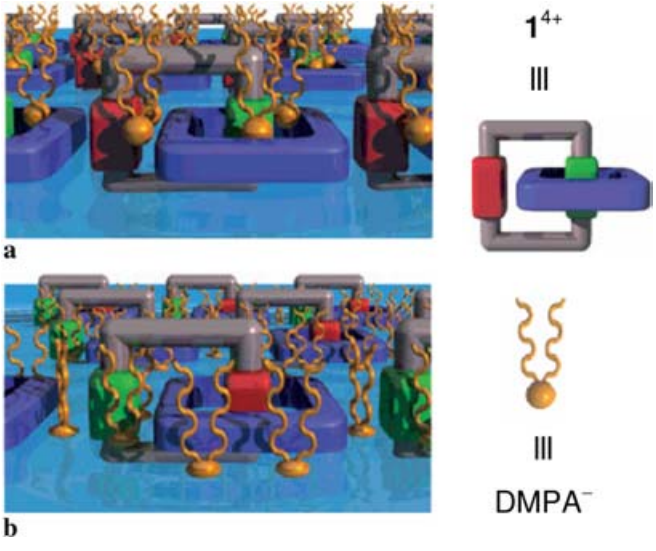

FIGURE 1 Graphical representation of the Langmuir monolayer of (**a**) $\mathbf{1}^{4+}/DMPA^{-}$ and (**b**) $\mathbf{1}^{6+}/DMPA^{-}$ system at the air-water interface, stabilized by intermolecular [π–π] stacking interactions between adjacent catenane molecules in the case of the former – and, in the case of the latter at higher pressures

ferent redox states in solution, can also be incorporated into Langmuir films, starting from either their tetracationic or chemically-oxidized hexacationic states. These films were transferred onto both mica and gold surfaces and their morphologies and current–voltage (I–V) characteristics were assessed and measured on these two surfaces. Not only are the morphologies of the films of these [2]catenanes in their different redox states, and therefore geometrical states, different [28], but their I–V behaviors are also dependent on the redox states of the [2]catenanes, prior to them being transferred onto gold. The tetracationic [2]catenanes exhibited smooth surfaces with a I–V behavior dominated by the tetracationic macrocycle component. By contrast, those monolayers containing the hexacationic [2]catenanes are less regular and exhibit a "metallic" I–V behavior.

Further investigations [5, 33, 34] by Brewster angle microscopy (BAM) and atomic force microscopy (AFM) of Langmuir monolayers of $\mathbf{1}^{4+}$ on silicon and $\mathbf{3}^{4+}$ on carbon nanotubes revealed the presence of supramolecular domains of the [2]catenane/$6\cdot\mathbf{4}^{-}$ lipid film, indicative of the phase separation of the pure $DMPA^{-}$ ($\mathbf{4}^{-}$) anions from the mixture of these anions with the [2]catenane. However, by varying the ionic strength of the subphase with added $CdCl_2$, the cross-sections of these domains were tunable from around 20 μm down to less than 3 μm. Divalent Cd^{2+} cations have been demonstrated [41] to lessen the electrostatic repulsion between the phospholipid headgroups. The reversibility of the redox switching displayed in solution by the [2]catenanes $\mathbf{1}^{4+}$, $\mathbf{2}^{4+}$ and $\mathbf{3}^{4+}$, coupled with the strategies that have been developed to deposit organized films onto surfaces, augured well for the use of these redox-active molecular switches in the design and fabrication of molecular electronic devices.

Molecular-electronics circuits based on crossbar architectures have been investigated. In a crossbar device, which can be used [9] for logic, sensing, signal routing, and memory applications, the molecular component is typically sandwiched [4] between two electrodes at the intersection of two crossing wires. Two-terminal MSTJs have been fabricated [5] based on the bistable [2]catenane $\mathbf{1}^{4+}$. The solid-state switching device consisted of a single monolayer of the [2]catenane, self-organized by their supporting amphiphilic $DMPA^{-}$ anions on the surface of a highly-doped n-type polycrystalline silicon (poly-Si) bottom electrode. To complete the MSTJ assembled device, a top electrode, consisting of titanium followed by aluminum, was deposited [5] onto the LB film using electron-beam evaporation through a shadow mask. Titanium was chosen as the top electrode on account of its known [42] high reactivity toward hydrocarbon chains, inhibiting the penetration of the subsequent metal atoms through the organic monolayer, shorting out the device.

The electrical signature of bistability for a two-terminal switch is that of hysteresis. Measurement of this hysteric response – called a remnant molecular signature – is obtained by using a particular voltage pulse sequence. In particular, the device is "written" at one voltage and the current is "read" at another voltage. The write and read voltages are applied sequentially. The former is scanned in 40 mV steps from 0 V out to +2 V, then back to −2 V, before returning to 0 V. However, the read voltage does not change (+0.1 V) and the current measurement, displayed along the y axis as the remnant molecular signature, is recorded during this "read" step. This experiment reveals opening (V_{open}) and closing (V_{close}) voltages, for switching between high and low conductance states, respectively. The devices incorporating the bistable $\mathbf{1}^{4+}$ [5] can be switched on at +2 V, off at −2 V, and read (junction resistance) between 0.1 and 0.3 V. And they may be cycled many times under ambient conditions. Moreover, the voltages required to open and close the switches were stable from one cycle to the next and from device-to-device. Various control devices demonstrated that the known bistability of the [2]catenanes $\mathbf{1}^{4+}$, $\mathbf{2}^{4+}$ and $\mathbf{3}^{4+}$, which is believed to arise from the relative mechanical mobilities of the macrocycles is critical for switching. In particular, for all the devices incorporating either eicosanoic acid **9**, $DMPA^{-}$ ($\mathbf{4}^{-}$) as its monosodium salt, the tetracationic macrocycle $\mathbf{5}^{4+}$ or the monostable degenerate [2]catenane $\mathbf{6}^{4+}$, hysteresis was not observed. Also binary switching signatures were absent when these controls were investigated under exactly the same conditions that were used for the bistable catenanes $\mathbf{1}^{4+}$, $\mathbf{2}^{4+}$ and $\mathbf{3}^{4+}$.

A molecule-based nanoelectromechanical switching mechanism has been proposed (Fig. 2), based on these findings. When the ground-state [A^0] of the [2]catenane is oxidized (by applying a bias of +2 V), the TTF unit (green)

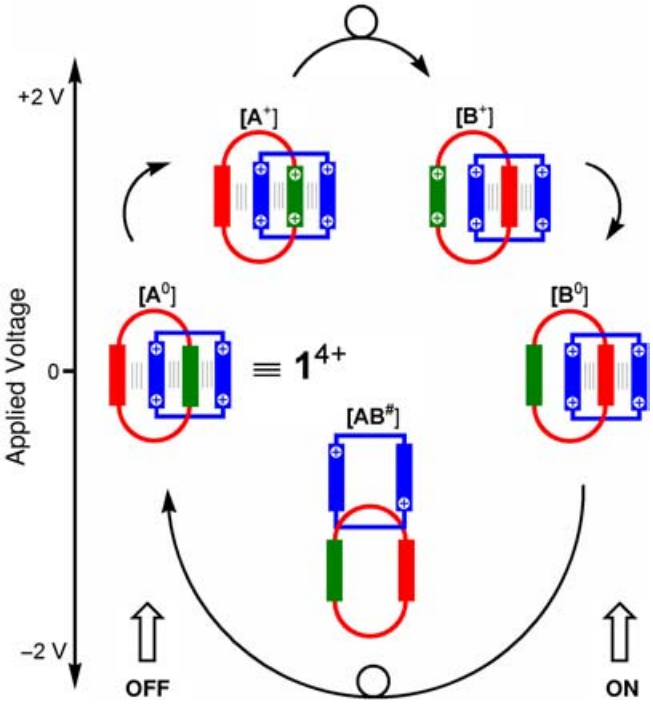

FIGURE 2 Graphical representation of the proposed nanoelectromechanical mechanism outlining the location of the tetracationic macrocycle for the OFF and ON state of the device. Co-conformer [A^0] represents both the ground-state of the [2]catenane and the "switch OFF" state of the device. When the [2]catenane is oxidized (by applying a bias of +2 V), the TTF groups (*green*) are ionized and experience a Coulomb repulsion with the tetracationic macrocycle (*blue*), resulting in the circumrotation of the ring and the formation of [B^+]. When the voltage is reduced to a near-zero bias, the metastable co-conformer [B^0] is formed. It represents the "switch ON" state of the device. Partial reduction of the cyclophane (at an applied bias of −2 V) is necessary to regenerate the [A^0] co-conformer. For simplicity of presentation, a $2e^-$ reduction step is shown, but the actual number of electrons was not measured, and so, the reduced form [$AB^{\#}$] is indicated with an unknown oxidation state

becomes positively charged – viz., $[A^+]$ and experiences a Coulomb repulsion with the tetracationic macrocycle (blue), resulting in the circumrotation of the ring and the formation of $[B^+]$ (Fig. 2). When the voltage is reduced to a near-zero bias, the metastable-state co-conformer $[B^0]$ is formed. This co-conformer of the ground-state $[A^0]$ was assigned to the "switch ON" state of the device. Partial reduction of the tetracationic macrocycle (at an applied bias of −2 V) is necessary to regenerate the $[A^0]$ ground-state co-conformer, which represents the "switch OFF" state of the device.

This mechanism is consistent [5] with temperature-dependent measurements of the device's operation, which indicate that the overall cycling of the switches has at least one thermally-activated step and is quenched near 230 K. In addition, as the device was cooled stepwise from 330 down to 230 K, the voltages required to open or close the switch systematically increased in magnitude. In single-molecule thick tunnel junctions, when the molecule is oxidized, the charge generated is balanced by image charges in the electrodes. At lower temperatures, the poly-Si electrode becomes less polarizable and therefore less able to support an image charge.

With the electromechanical mechanism enjoying strong experimental support (vide infra) and the need to miniaturize MSTJs as a means to realize their placement at the nanometer length scale "beyond CMOS", we identified [34] a bistable catenane molecule for a single-walled carbon nanotube (SWNT)-based device (Fig. 3a). Since the catenane occupies about a nanometer cube, it fits neatly onto the roughly one nanometer diameter of SWNTs. The decision to use SWNTs in such a device was driven by their overall properties – namely stability against oxidation and high carrier mobility – and not just because of their nanoscale dimensions [43]. The device was fabricated around the bistable [2]catenane $\mathbf{3}^{4+}$ in which diazapyrenium units replace the bipyridinium ones in the tetracationic macrocycle of $\mathbf{1}^{4+}$.

MSTJs incorporating SWNT bottom electrodes were found to operate in a manner that is strikingly similar to the situation when the bottom electrode is poly-Si. The $\mathbf{3}^{4+}/6\cdot\mathbf{4}^{-}$-assembled MSTJ device exhibited hysteresis with a "read" current difference (Fig. 3b) of nearly a factor of four. In fact, active and remnant I–V measurements demonstrated (Fig. 3c) that these devices can be switched reconfigurably and cycled repeatedly between high and low current states under ambient conditions. In this work, two controls were utilized – one based on the plain tetracationic macrocycle $\mathbf{7}^{4+}$ and the other on a degenerate, non redox-active catenane $\mathbf{8}^{4+}$. Neither of these control devices yielded electronic switching. Thus, once again, we attributed the bistable character of these working solid-state devices as arising from hysteretic electromechanical motions in the redox-switchable interlocked molecules. In fact, all of the device characteristics were preserved from those first observed on the poly-Si electrode, providing further support for the electrochemical switching mechanism proposed [5] back in 2000 for a bistable catenane in solid-state devices.

The redox-switching phenomenon associated with bistable [2]catenane has also been observed [16, 24] for bistable [2]rotaxanes in the solution phase. Thus, if the bistability associated with the MSTJs is truly molecular in origin, then the same properties should emerge from devices incorporating bistable [2]rotaxanes. We will now describe how the electromechanical switching mechanism has been shown to carry over into solid-state devices when amphiphilic bistable rotaxanes constitute the molecular monolayers in the crossbars of the MSTJs.

3 Rotaxanes in monolayers

The bistable [2]rotaxanes $\mathbf{10}^{4+}$–$\mathbf{15}^{4+}$ (Scheme 4) are another class of mechanically interlocked molecules that have been exploited [4, 44–47] comprehensively – together

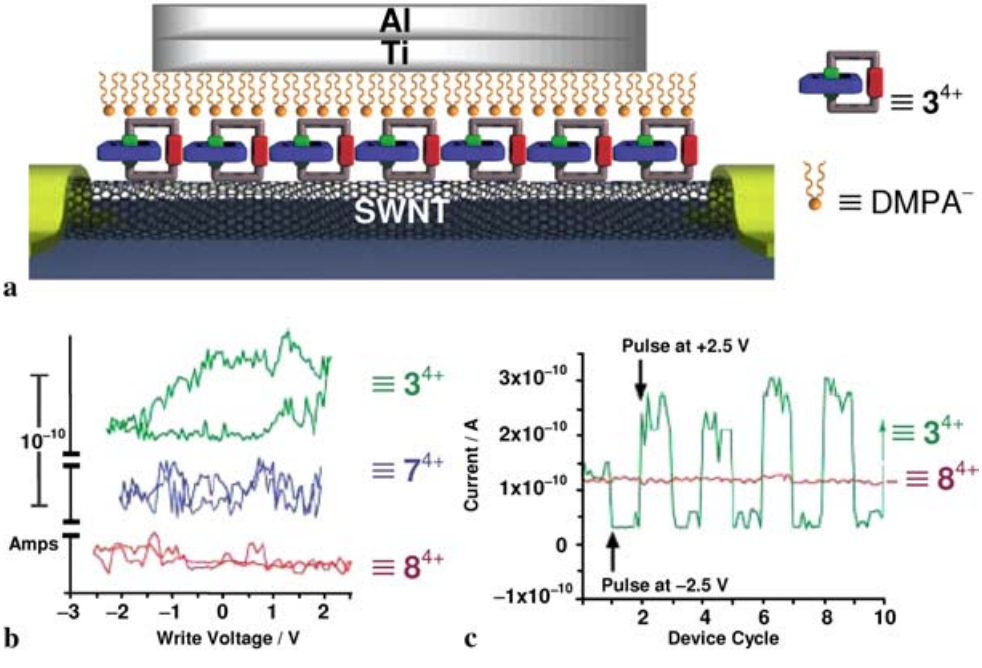

FIGURE 3 (**a**) Graphical representation of a single monolayer of a bistable [2]catenane $\mathbf{3}^{4+}$, that was anchored with amphiphilic phospholipid counterions and sandwiched between a semiconducting SWNT and a Ti/Al top electrode. (**b**) Remnant molecular signatures for the devices containing the bistable [2]catenane $\mathbf{3}^{4+}$, and appropriate controls, such as the tetracationic macrocycle $\mathbf{7}^{4+}$ and the degenerate [2]catenane $\mathbf{8}^{4+}$. The read voltage for these three traces was 100 mV. (**c**) Device cycling for the bistable [2]catenane $\mathbf{3}^{4+}$ contrasted with the lack of cycling for the degenerate [2]catenane $\mathbf{8}^{4+}$. In both cases, V_{read} was 100 mV, V_{open} was +2.5 V and V_{close} was −2.5 V

with their dumbbell counterparts **16**–**21** – for the construction of solid-state devices. Just as we have witnessed for bistable catenanes, it is essential that we establish how to self-assemble bistable rotaxanes in an orderly manner at interfaces and on surfaces. Several studies have been devoted to introducing rotaxanes onto surfaces, either by means of SAMs [31] or as LB films [30, 32]. For SAMs, the disulfide moiety has been used as the surface active headgroup on redox-active [2]rotaxanes (e.g., $\mathbf{10}^{4+}$ and $\mathbf{11}^{4+}$) for attachment onto gold [31] and platinum [44] surfaces. Although SAMs provide a chemically more stable bond between the rotaxane and metal surfaces, LB monolayers have the advantage that they can be deposited on almost any kind of solid substrate [38–40].

The formation of LB monolayers has been achieved by introducing hydrophilic headgroups as a means of producing [48] amphiphilic redox-switchable [2]rotaxanes (e.g., $\mathbf{12}^{4+}$, $\mathbf{13}^{4+}$, $\mathbf{14}^{4+}$ and $\mathbf{15}^{4+}$). By contrast with the bistable [2]catenanes, Langmuir film formation of amphiphilic rotaxanes did not exhibit [33] a dependence upon the nature of the subphase ($CdCl_2$). In order to optimize the redox stability of the amphiphilic bistable rotaxanes on surfaces, a systematic study [30] investigating the effect of changing the hydrophilic stopper in the [2]rotaxanes has been carried out. A series of amphiphilic bistable [2]rotaxanes based on $\mathbf{12}^{4+}$ have been designed and synthesized [30]. The amphiphilic dumbbell component is terminated by a hydrophobic tetraarylmethane-based stopper (near the TTF unit) at one end and by a hydrophilic tetraarylmethane-based stopper (near the DNP ring system) at the other end. The effects of systematic changes in the constitutions and therefore the hydrophilicities of the three ethylene glycol tails (diethylene or tetraethylene glycol), and upon the end groups (hydroxyl or methoxyl functions) attached to the hydrophilic stoppers, on the Langmuir monolayer stabilities, co-conformations and superstructures of the [2]rotaxanes and their dumbbell counterparts were examined [30]. In general, greater hydrophilic strength – i.e., the presence of the tetracationic macrocycle component and hydroxyl end groups on the anchor stopper – leads to a higher stability and viscoelasticity of the film. Molecular conformations within the films were also shown to be influenced by the hydrophilic tail length (diethylene or tetraethylene glycol). For a short hydrophilic tail (diethylene glycol) as in $\mathbf{12}^{4+}$, the π-A isotherm showed (Fig. 4a) two well-defined regions, a low-pressure liquid-expanded (LE) region followed by a transition shoulder to a liquid-condensed (LC) region. From the π-A isotherm (Fig. 4a) of the corresponding dumbbell counterpart **18**, it is evident that the tetracationic macrocycle has a significant effect on the isotherm's behavior. These studies allowed us to propose (Fig. 4b) a model for the superstructures of these particular rotaxanes, $\mathbf{12}^{4+}$ and iso-$\mathbf{12}^{4+}$ – of which the former was used in subsequent MSTJ devices – at different surface pressures. At low pressures, the tetracationic macrocycle competes effectively with short diethylene glycol tails for anchoring the rotaxane in the subphase, leading to a folded or tilted conformation. At the transition pressure ($\sim 30\,\mathrm{mN/m}$), the proximity of the rotaxanes induces them to stand vertically throughout the LC phase. When the longer tetraethylene glycol tails are present, such a transition is not observed directly in the isotherm. In this case, it is believed that the tail-to-tail intermolecular interactions dominate affinity for the water subphase, and so, the molecule's conformation is less affected by the tetracationic macrocycle.

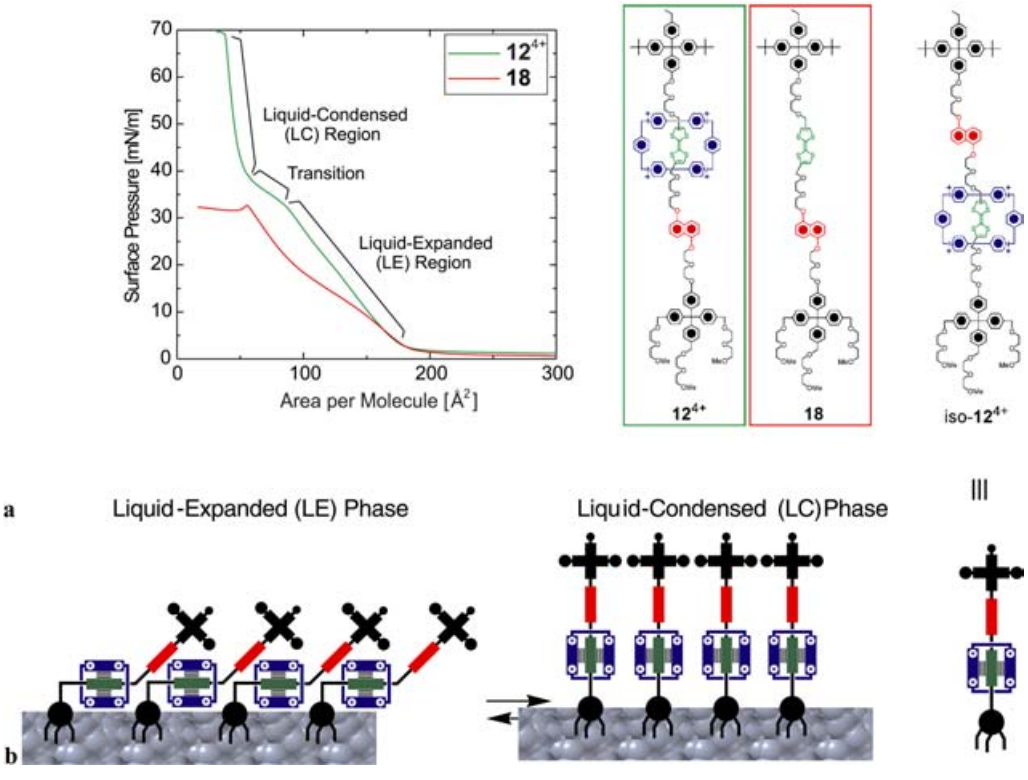

FIGURE 4 (**a**) π-A isotherms recorded at 20 °C for $\mathbf{12}^{4+}$ and **18**, with the different regions of the isotherm labeled. (**b**) Schematic representation of the proposed molecular conformations of the [2]rotaxane $\mathbf{12}^{4+}$ Langmuir films. These films typically pass from a liquid-expanded (LE) region, wherein the molecules display some degree of conformational folding to a liquid-condensed (LC) region, at which point the [2]rotaxane iso-$\mathbf{12}^{4+}$ stand perpendicular to the substrate

The movement of the tetracationic macrocycle component of the bistable amphiphilic [2]rotaxanes $\mathbf{13}^{4+}$ and $\mathbf{14}^{4+}$ in closely packed Langmuir and LB films was verified [49] using X-ray photoelectron spectroscopy (XPS). The photoemission intensity of each element depends on the depth within the monolayer at which the photoelectron is emitted and, in particular, it attenuates exponentially with increased depth. Therefore, the XPS technique can be used to differentiate atoms at different depths within a film. In other words, molecular shuttling can be monitored by using XPS to track the nitrogen (N) atoms which are present solely in the bistable rotaxane's only moving part, the tetracationic macrocycle component. Both the starting state $\mathbf{13}^{4+}$, and the oxidized rotaxane $\mathbf{13}^{6+}$, were analyzed (Fig. 5) by XPS. A higher intensity for the N (1*s*) peak was observed in the oxidized rotaxane film $\mathbf{13}^{6+}$ than in the starting state $\mathbf{13}^{4+}$, an observation which supports the hypothesis that, in the oxidized rotaxane, the ring had moved from the dicationic TTF^{2+} site to encircle the DNP recognition site, placing it closer to the film's surface. Control experiments conducted using the rotaxane $\mathbf{14}^{4+}$, in which the positions of the TTF and DNP sites are reversed compared to those in $\mathbf{13}^{4+}$, ruled out the possibility of an oxidation-induced change in the N density, as well as the influence of the rotaxane's unfolding. These XPS studies were supported [49] by π-A isotherm analysis, which show that the switching of the macrocycle component of the bistable amphiphilic [2]rotaxane $\mathbf{13}^{4+}$ causes significant changes to the occupied area of the rotaxane. Comparing their starting and oxidized states under the same pressure, it was observed that the projected mean molecular areas for $\mathbf{13}^{4+}$ in the LE phase increases from 2.8 nm^2/molecule to become 3.2 nm^2/molecule for the oxidized rotaxane $\mathbf{13}^{6+}$.

To achieve a better understanding of the electromechanical mechanism associated with the switching in the rotaxane-based SAMs, electrochemical investigations were performed on a disulfide-tethered bistable rotaxane $\mathbf{10}^{4+}$ SAM on gold [31]. A nanoelectromechanical mechanism (Fig. 6a) has been proposed [31] to account for the half-device's observed experimental behavior. The ground-state corresponds to the translational isomer with the tetracationic macrocycle encircling the TTF unit. On applying a +630 mV voltage, the TTF unit becomes oxidized ($TTF^{+\bullet}$ or TTF^{2+}) and, just as in solution, the resulting charge-charge repulsive force drives a linear movement of the tetracationic macrocycle along the dumbbell component to encircle the DNP ring system. When the voltage is removed, neutrality is restored to the TTF unit and yet the tetracationic macrocycle remains around the DNP ring system, forming a metastable state. The ring's location can be reset by applying a potential of −600 mV, so returning the macrocycle back to the TTF unit and the SAM of the rotaxane back to its ground-state. Otherwise, one has to wait for up to many minutes for the metastable state to decay thermally back to the ground state.

Cyclic voltammetric measurements carried out at different scan rates have also demonstrated [31] that the kinetics associated with the first order decay (Fig. 6b) of the metastable state back to the ground-state cover a range of lifetimes (τ) – from 1.3 s at 303 K to ca. 5 min at 263 K – in keeping with an activation barrier of 17.7 kcal mol^{-1} for the decay of the metastable state back to the ground-state. Or, as we noted above, the metastable state can be regenerated instantaneously by reducing the tetracationic macrocycle. The samples retained their electrochemical robustness over the course of several days in the electrolyte.

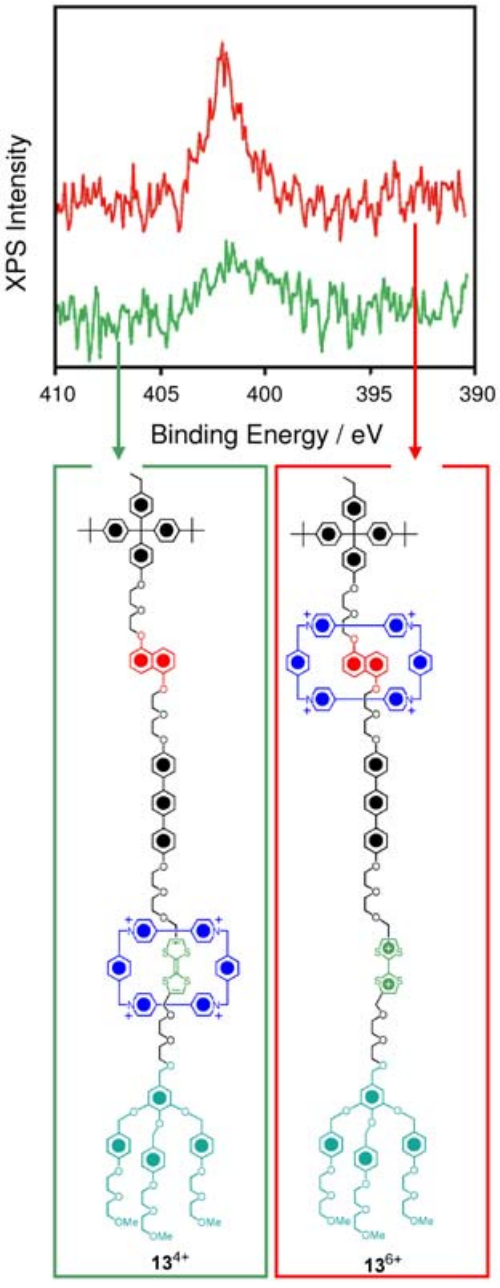

FIGURE 5 Nitrogen (1*s*) X-ray photoemission spectra for the starting-state rotaxane $\mathbf{13}^{4+}$ (*green line*) and its oxidized form $\mathbf{13}^{6+}$ (*red line*). The different N (1*s*) peak areas is attributed to the switching of the ring component from one station to the other in self-organized, closely packed LB monolayers

4 Rotaxanes in devices

In rotaxane-based devices, the active device elements in MSTJs are [4] self-organized LB monolayers of the amphiphilic bistable [2]rotaxanes $\mathbf{15}^{4+}$, sandwiched between poly-Si wires and top electrodes of titanium, topped with aluminum in a crossbar device architecture (Fig. 7a). The rem-

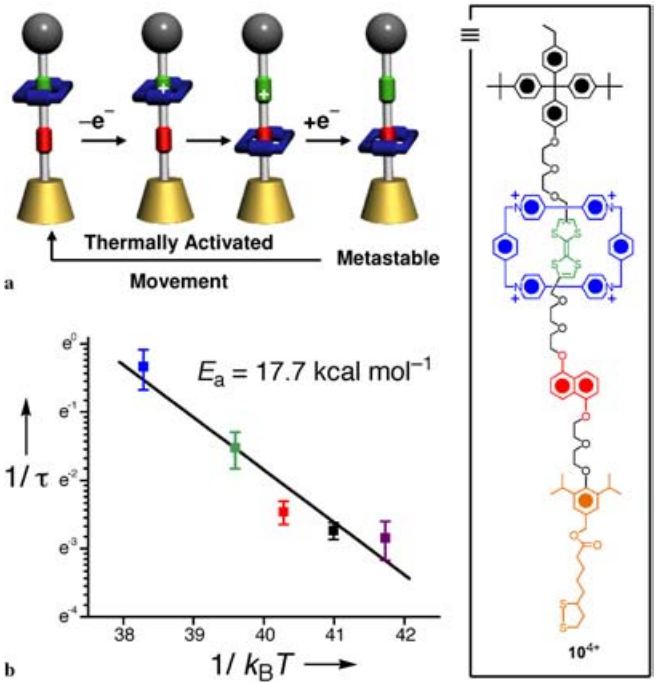

FIGURE 6 (**a**) Proposed nanoelectromechanical switching mechanism of the [2]rotaxane $\mathbf{10}^{4+}$ self-assembled onto a gold surface in the form of a half-device. The proposed mechanism differs from that of [2]catenanes only in that the [2]rotaxane undergoes a linear mechanical motion rather than a circumrotation. (**b**) An Arrhenius plot of $(1/\tau)$ against $(1/k_BT)$, from which an activation energy (E_a) of 17.7 ± 2.8 kcal mol^{-1} has been obtained for the relaxation process

nant molecular signature (Fig. 7b) and the binary switching behavior (Fig. 7c) indicate that the switch-ON (high conductance) and switch-OFF (low conductance) states of each junction can be addressed respectively upon applying a +2 V or a −2 V bias. The metastability observed in this rotaxane-based device also supports the redox-controlled electromechanical switching mechanism proposed [31] to account for the switching in half-devices. The device is observed to decay to the OFF state in a manner that is qualitatively similar to the movements of the tetracationic macrocycle in rotaxanes that are self-assembled onto a gold electrode. Therefore, the decay rate is a function of the thermally activated linear movement of the tetracationic macrocycle back along the dumbbell to the TTF unit. Alternatively, applying a reverse bias of −2 V causes the electrochemical reduction of the tetracationic macrocycle, allowing the facile reformation of the more stable translational isomer.

The proposed switching mechanism, while based on the molecule's mechanical movements – known [16, 24, 31] to occur in solution and in SAMs – is supported experimentally by comparisons with control devices. In particular, devices utilizing the dumbbell-only compound **21**, and non-redox active molecules such as eicosanoic acid **9**, do not display any switching behavior.

5 A universal switching mechanism

In yet more recent experiments, the switching dynamics of bistable [2]catenanes and [2]rotaxanes within a variety of physical environments, including a solid-state polymer electrolyte gel [50] and the solution phase [51], have been investigated. These studies, combined with previous studies on a half-device and full devices, have revealed that the kinetic and thermodynamic parameters of the switching mechanism changes quite dramatically from one environment to another. More important, however, is the fact that, while these parameters exhibit a strong environmental dependence, a single, generic switching mechanism is observed for all the bistable

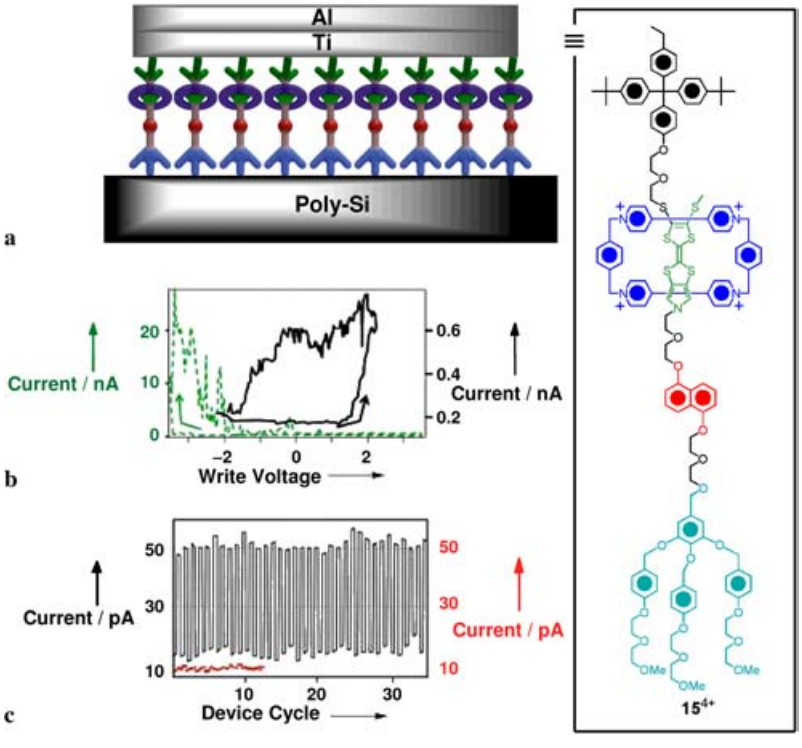

FIGURE 7 Nanoelectronic devices have been constructed from the bistable rotaxane $\mathbf{15}^{4+}$. (**a**) Graphical representation of $\mathbf{15}^{4+}$ sandwiched between two electrodes. (**b**) Molecular remnant signature of $\mathbf{15}^{4+}$ (*black*) and the dumbbell-only control molecule **21** (*green*). (**c**) Binary switching behavior of the device based on $\mathbf{15}^{4+}$ (*black*), switched to high current at +2 V and to low current at −2 V, and of the control device based on **9** (*red*). The *black trace* in (**c**) represents 35 cycles of the nanometer-scale device, recorded by repeatedly closing and opening the switch, and then monitoring the current through the junction, at 0.1 V applied bias, after each writing event

molecules, regardless of whether they are in liquid solution, immobilized within a liquid polymer matrix or tethered to a solid support.

6 Molecular signatures emerging out of the physical background

The operational molecular devices outlined so far in this review are all built around one specific electrode-molecule-electrode configuration that utilizes a semiconducting Si or C bottom electrode with an LB monolayer of bistable molecules and a metallic Ti/Al top electrode. It was this particular configuration that has allowed the measurement of a conductance signal that arises in direct response to the passage of an electrical current through the molecular switches. This situation is somewhat reminiscent of how very precise information on molecular structure, in the form of what chemists refer to today as chemical shifts and coupling constants, began to emerge slowly half a century ago out of the technique of nuclear magnetic resonance (NMR) spectroscopy uncovered by physicists [52]. In the early days, it was possible, for example, to observe a broad signal in the radiofrequency region of the electromagnetic spectrum for hydrogen atoms (protons) in an organic compound when a sample was probed in an NMR spectrometer at some relatively low magnetic field, e.g., 25 MHz. As instrumentation improved, the magnitude of this operating magnetic field was increased and very much better field homogeneities were attained, the broad signals became increasingly well resolved and contained more molecularly sensitive information, e.g., coupling constants (< 1–25 Hz) between protons (revealing bond distance and geometry dependences) on a chemical shift scale of around 10 parts per million (ppm), e.g., 600 Hz for each ppm at an operating field of 600 MHz on the part of a good modern-day high-field NMR spectrometer. The practice could be likened in the world at large to looking for a needle in haystack!

The same relative level of performance [53] is being demanded from electronic devices in order to allow their molecular signatures to emerge from out of all other sources of background current-flow. During our research on molecular electronics devices, an activity which includes break junctions [44] and alternative device settings [45–47] using wholly metallic electrodes, we have identified [9] that, for the class of molecular switches we have developed, at least one of the electrodes has to be composed of elements clustered around carbon, hydrogen and nitrogen in the Periodic Table in order for the molecular signal to be observed against a lot of potential background.

In the context of a single-molecule transistor, break junctions coupled with a third gate electrode, have been fabricated [44] using rotaxanes. The gate provides an electrical field for tuning the molecular-electronic energy levels into and out of resonance with the Fermi energies of the source and drain electrodes. In this type of single-molecule device, the molecule behaves as a structurally flexible quantum dot, resulting in a resonant tunneling transistor-type device. Since measurements were conducted at 4 K, there is no molecular mechanical movement of the tetracationic macrocycle.

We have investigated single-molecule transistor devices [44], based on bridging the bistable [2]rotaxanes $\mathbf{10}^{4+}$ and $\mathbf{11}^{4+}$ (and various control compounds) between (Fig. 8a) two Pt break-junction electrodes. While $\mathbf{11}^{4+}$ can form, on both sides, bonds based on chemisorption between the five-membered disulfide rings and the platinum electrodes, the tetraarylmethane stopper at one end of $\mathbf{10}^{4+}$ can only become physisorbed onto a platinum electrode.

In contrast with the devices based on poly-Si or SWNT bottom electrodes, differential conductance measurements revealed (Fig. 8b–e) that the I–V signatures observed are dominated by the interface between the molecules ($\mathbf{10}^{4+}$ and $\mathbf{11}^{4+}$) and the Pt electrodes, rather than by the internal electronic structures of the rotaxanes. This interpretation follows from the observed symmetry in the differential conductance measurements. While, in the case of $\mathbf{11}^{4+}$ a symmetric signature was observed, $\mathbf{10}^{4+}$ exhibited an asymmetric signature. If, however, electron transport was dominated solely by the bistable rotaxane molecules, the signature would be expected to be asymmetric in both cases. This observation draws attention to the importance of considering the molecule and the electrode as a single non-separable entity. In order to observe a molecular signature, the background current associated with the interface must not swamp the conductance signal arising from the molecule.

Further studies on nanoscale molecular-electronic devices, comprised of an LB monolayer of bistable [2]rotaxanes

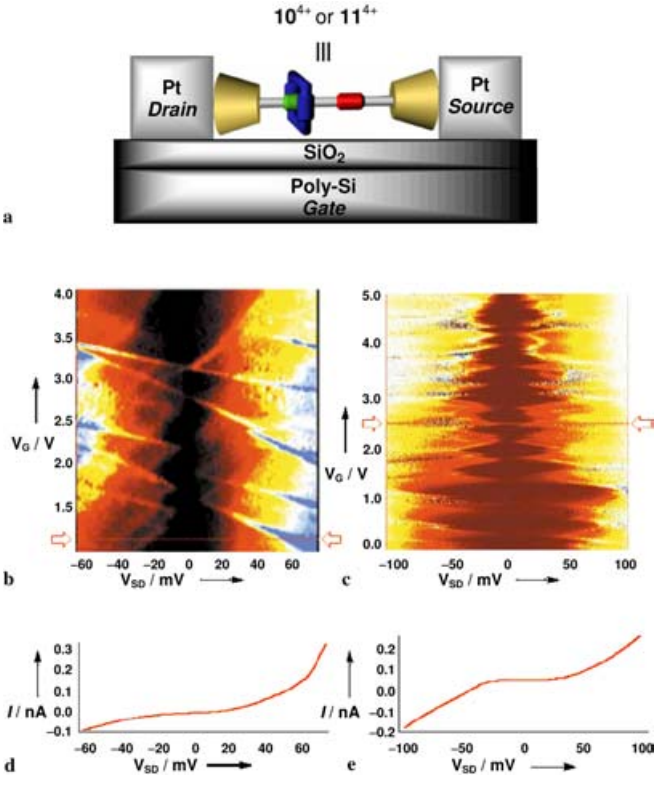

FIGURE 8 (**a**) Graphical representation of a three-terminal device with a bistable [2]rotaxane ($\mathbf{10}^{4+}$ or $\mathbf{11}^{4+}$) bridging the gap between a Pt break-junction source and drain electrodes. Differential conductance ($\mathrm{d}I/\mathrm{d}V$) plot for [2]rotaxane (**b**) $\mathbf{10}^{4+}$ and (**c**) $\mathbf{11}^{4+}$. The color represents the $\mathrm{d}I/\mathrm{d}V$ of the junction, with the darkest areas in the center of the plot indicating the regions of no current. Current–voltage (I–V) curves for [2]rotaxane (**d**) $\mathbf{10}^{4+}$ and (**e**) $\mathbf{11}^{4+}$. The I–V curves shown in (**d**) and (**e**) were taken at the gate voltages (V_G) indicated by the red arrows located at the sides of (**b**) and (**c**)

sandwiched between wholly metal electrodes, such as Ti/Pt-Ti/Pt [45, 46] and Pt-Ti/Al [47], also revealed a generic switching mechanism. Yet, it is not one which is based on molecular bistability, but rather one which is dominated by either the properties of the electrodes or the electrode-molecule interfaces. Although such devices are bistable, they display massive currents and large current ratios of $\sim$ 10000:1 compared with the 5:1 ratios for Si-based devices. Also, they exhibited no temperature-dependence. Furthermore, it is likely that, any molecule which forms a stable monolayer can display the same effect, – i.e., these devices, while bistable and nanoscaled, are completely blind to the nature of the molecule.

Organic-metal interactions are typically polar, a propriety which implies [54] that, at zero bias, some charge must flow between the molecule and the electrodes to equilibrate the chemical potential across the junction. This phenomenon can also modify the electronic character of the molecule, giving rise to Schottky-like barriers to charge flow across electrode/molecule interfaces. Such barriers, which can partially or fully mask the molecule's electronic signature, increase with larger electronegativity differences. For this reason, and others – including stability, reproducibility, and generality – interfacial chemical interactions involving carbon, silicon, and oxygen atoms may well be preferred [9] over organic-metal interfaces, such as gold or platinum with sulfur in many nanoelectronic devices.

7 Modeling and simulation of rotaxanes and devices

Recent computational studies [55] have focused on a model of the device in its entirety, as well as the molecular component of the device – in particular, the electronic structure-derived [56] density-of-states (DOS) of the rotaxane's TTF, DNP and $CBPQT^{4+}$ units and the superstructures [57] of rotaxanes in SAMs on gold. These endeavors provide a basis on which to understand device behavior and on which to make new molecules and devices by rational design.

In a model system composed of a single pseudorotaxane (i.e., a rotaxane without stoppers) that was sandwiched between electrodes represented by three gold atoms each, the *I–V* curves were simulated [55] for the ground and metastable state co-conformations. Using first principles calculations, the high conductance state is observed when the tetracationic macrocycle is located around the DNP unit – a finding that is consistent with the originally proposed mechanism [5]. It has been suggested that the more delocalized molecular orbitals, as well as the smaller energy gap between the highest occupied molecular orbital (HOMO) and lowest unoccupied molecular orbital (LUMO), are the major factors leading to the higher conduction of the metastable state co-conformation.

The electronic structure of a [2]rotaxane, constructed by combining the energy levels of the separate stations (TTF and DNP) with and without a $CBPQT^{4+}$ macrocycle encircling them, was characterized [56] in more detail utilizing ab initio quantum mechanical methods. These results indicate that the energies of the HOMO of the TTF and DNP unit shift to lower energy – the former move more so than the latter – when the tetracationic macrocycle encircles one of them. In addition, the modeling revealed that the co-conformation that generates the more highly conducting device is also dependent on the molecule's conformation. It turns out that, if the molecule exists in a folded conformation, higher conduction is predicted to occur when the macrocycle encircles the DNP unit, i.e., when the molecule is in its high conductance co-conformation, according to both experiment and calculation.

Simulations of SAMs of the bistable [2]rotaxane $\mathbf{10}^{4+}$ were undertaken [57] in order to understand what the superstructure and conformation of rotaxanes resemble when they are close-packed at the surface coverages employed in the MSTJ device preparations. It was found that, at a mean molecular area of 1.4 nm^2/molecule, the rotaxane is folded such that, in the high conductance co-conformation, the tetracationic macrocycle, although encircling the DNP unit, is also close to, if not interacting in a side-on fashion with, the TTF unit. Furthermore, two empirical observations support the presence of folded superstructures. The studies [30] on Langmuir monolayers suggested folded structures (Fig. 4), as a consequence of the tetracationic macrocycle's affinity for the water subphase at $\sim$ 1.5 nm^2/molecule. Secondly, the simple observation [4, 5] that MSTJ devices, incorporating bistable catenanes and rotaxanes, display similar hysteresis in the remnant molecular signatures and ON/OFF current ratio's of $\sim 5:1$ implies that the superstructures of the catenanes and rotaxanes are quite similar. Such a conclusion is consistent with a folded conformation for the rotaxanes. Although more modeling and simulations needs to be performed, the results to date are consistent with the mechanism we currently prefer as an explanation for the experimental results. More importantly, the computational results have revealed how the superstructures, conformations and co-conformations influence the properties of the MSTJ devices, and so help us to identify important factors when considering the design of the next generation of bistable molecules for MSTJs.

8 Summary and outlook

In conclusion, only bistable catenanes and rotaxanes, which operate as electrochemically driven, molecular-mechanical switches in solution, or as self-assembled monolayers on gold electrodes, display binary switching behavior in solid-state device settings. The molecule-based switching mechanism is supported by systematic control experiments. Specifically, (1) degenerate catenanes, (2) tetracationic macrocycle-only components, (3) redox-addressable, dumbbell-only counterparts rotaxanes, and (4) linear non-redox addressable compounds do not yield remnant molecular signatures, either in the solution phase or in device settings. The observation of electromechanical switching of the tetracationic macrocycle between 'stations' in bistable rotaxanes mounted on solid substrates as LB films, together with the presence of metastability in half-devices, as well as in full devices, lends strong support to the proposed electromechanical switching mechanism. This behavior is in stark contrast to the operation of devices that utilize wholly metal bottom electrodes, such as gold or platinum. In those devices, the majority of the signal arises from current that flows directly in response to the metal interface generating sufficient background current to obliterate the molecule's signature. The all-important problem that now needs to be tackled and solved is how to

develop robust fabrication methods to realize devices in a routine manner. In addition, further simulation and modeling is needed to bridge the gap from the design, synthesis and operation of molecules in solution to their performance in solid-state devices.

ACKNOWLEDGEMENTS The authors acknowledge support of this work by the Office of Naval Research (ONR), the National Science Foundation (NSF), the Moletronics Program of the Defense Advanced Research Projects Agency (DARPA), the Microelectronics Advanced Research Corporation (MARCO) its Focus Center on Functional Engineered NanoArchitectonics (FENA), and the Center for Nanoscale Innovation for Defense (CNID).

REFERENCES

1 a) S.W. Han, I. Lee, K. Kim: Langmuir **18**, 182 (2002); b) M.J. Tarlov, Jr D.R.F. Burgess, G. Gillen: J. Am. Chem. Soc. **115**, 5305 (1993); c) J. Huang, D.A. Dahlgren, J.C. Hemminger: Langmuir **10**, 626 (1994); d) K.C. Chan, T. Kim, J.K. Schoer, R.M. Crooks: J. Am. Chem. Soc. **117**, 5875 (1995); e) P.B. Fischer; S.Y. Chou: Microelectron. Eng. **21**, 311 (1993); f) I.W. Rangelow, Z. Borkowicz, P. Hudek, I. Kosti: Microelectron. Eng. **25**, 49 (1994); g) M. Despont, U. Staufer, C. Stebler, R. Germann, P. Vettiger: Microelectron. Eng. **27**, 467 (1995)

2 V. Balzani, A. Credi, F.M. Raymo, J.F. Stoddart: Angew. Chem. Int. Ed. **39**, 3348 (2000)

3 a) M. Schulz: Nature **399**, 729 (1999); b) D.A. Muller, T. Sorsch, S. Moccio, F.H. Baumann, K. Evans-Lutterodt, G. Timp: Nature **399**, 758 (1999); c) D. Goldhaber-Gordon, M.S. Montemerlo, J.C. Love, G.J. Opiteck, J.C. Ellenbogen: Proceedings of the IEEE **85**, 521 (1997)

4 Y. Luo, C.P. Collier, J.O. Jeppesen, K.A. Nielsen, E. Delonno, G. Ho, J. Perkins, H.-R. Tseng, T. Yamamoto, J.F. Stoddart, J.R. Heath: Chem Phys Chem. **3**, 519 (2002)

5 C.P. Collier, G. Mattersteig, E.W. Wong, Y. Luo, K. Beverly, J. Sampaio, F.M. Raymo, J.F. Stoddart, J.R. Heath: Science **289**, 1172 (2000)

6 A. Seth, T. Otomo, H.L. Yin, M.K. Rosen: Biochemistry **42**, 3998 (2003)

7 J. Kalinowski, M. Cocchi, G. Giro, V. Fattori, P. Di Marco: J. Phys. D: Appl. Phys **34**, 2274 (2001)

8 a) A. Troisi, M.A. Ratner: Nano Lett. **4**, 591 (2004); b) T. Xu, I.R. Peterson, M.V. Lakshmikantham, R.M. Metzger: Angew. Chem. Int. Ed. **40**, 1749 (2001)

9 J.R. Heath, M.A. Ratner: Physics Today **56**, 43 (2003)

10 http://www.zettacore.com/

11 A.H. Flood, R.J.A. Ramirez, W.-Q. Deng, R.P. Muller, W.A. Goddard III, J.F. Stoddart: Aust. J. Chem. **57**, 301 (2004)

12 V. Balzani, A. Credi, F.M. Raymo, J.F. Stoddart: Angew. Chem. Int. Ed. **39**, 3348 (2000)

13 M.C.T. Fyfe, J.F. Stoddart: Acc. Chem. Res. **30**, 393 (1997)

14 a) G. Schill: *Catenanes, Rotaxanes, and Knots* (Academic Press, New York 1971); b) D.B. Amabilino, J.F. Stoddart: Chem. Rev. **95**, 2725 (1995); c) D. Philp, J.F. Stoddart: Angew. Chem. Int. Ed. Engl. **35**, 1154 (1996); d) J.-P Sauvage, C. Dietrich-Buchecker: *Molecular Catenanes, Rotaxanes and Knots* (Wiley-VCH, Weinheim 1999)

15 V. Balzani, A. Credi, G. Mattersteig, O.A. Matthews, F.M. Raymo, J.F. Stoddart, M. Venturi, A.J.P. White, D.J. Williams: J. Org. Chem. **65**, 1924 (2000)

16 H.-R. Tseng, S.A. Vignon, J.F. Stoddart: Angew. Chem. **115**, 1529 (2003); Angew. Chem. Int. Ed. **42**, 1491 (2003)

17 a) P.-L. Anelli, N. Spencer, J.F. Stoddart: J. Am. Chem. Soc. **113**, 5131 (1991); b) P.-L. Anelli, M. Asakawa, P.R. Ashton, R.A. Bissell, G. Clavier, R. Górski, A.E. Kaifer, S.J. Langford, G. Mattersteig, S. Menzer, D. Philp, A.M.Z. Slawin, N. Spencer, J.F. Stoddart, M.S. Tolley, D.J. Williams: Chem. Eur. J. **3**, 1113 (1997); c) D.A. Leigh, A. Troisi, F. Zerbetto: Angew. Chem. **112**, 358 (2000); Angew. Chem. Int. Ed. **39**, 350 (2000)

18 a) C.O. Dietrich-Buchecker, J.-P. Sauvage, J.-M. Kern: J. Am. Chem. Soc. **106**, 3043 (1984); b) C.O. Dietrich-Buchecker, J.-P. Sauvage, Tetrahedron **46**, 503 (1990); c) M.J. Gunter, M.R. Johnston: J. Chem. Soc. Chem. Commun., 829 (1994); d) M.-V. Martínez-Díaz, N. Spencer, J.F. Stoddart: Angew. Chem. Int. Ed. Engl. **36**, 1904 (1997); e) T.R. Kelly, H. De Silva, R.A. Silva: Nature **401**, 150 (1999); f) A.M. Elizarov, S.-H. Chiu, J.F. Stoddart: J. Org. Chem. **67**, 9175 (2002)

19 R.A. Bissell, E. Córdova, A.E. Kaifer, J.F. Stoddart: Nature **369**, 133 (1994)

20 M. Asakawa, P.R. Ashton, V. Balzani, A. Credi, C. Hamers, G. Mattersteig, M. Montalti, A.N. Shipway, N. Spencer, J.F. Stoddart, M.S. Tolley, M. Venturi, A.J.P. White, D.J. Williams: Angew. Chem. Int. Ed. **37**, 333 (1998)

21 a) P.R. Ashton, R. Ballardini, V. Balzani, M.T. Gandolfi, D.J.-F. Marquis, L. Pérez-García, L. Prodi, J.F. Stoddart, M. Venturi: J. Chem. Soc. Chem. Commun. 177 (1994); b) A. Livoreil, C.O. Dietrich-Buchecker, J.-P. Sauvage: J. Am. Chem. Soc. **116**, 9399 (1994); c) P.R. Ashton, R. Ballardini, V. Balzani, A. Credi, M.T. Gandolfi, S. Menzer, L. Pérez-García, L. Prodi, J.F. Stoddart, M. Venturi, A.J.P. White, D.J. Williams: J. Am. Chem. Soc. **117**, 11 171 (1995); d) F. Baumann, A. Livoreil, W. Kaim, J.-P. Sauvage: Chem. Commun., 35 (1997); e) L. Raehm, J.-M. Kern, J.-M. Sauvage: Chem. Eur. J. **5**, 3310 (1999); f) R. Ballardini, V. Balzani, W. Dehaen, A.E. Dell'Erba, F.M. Raymo, J.F. Stoddart, M. Venturi: Eur. J. Org. Chem., 591 (1999); g) P. Ceroni, D.A. Leigh, L. Mottier, F. Paolucci, S. Roffia, D. Tetard, F. Zerbetto: J. Phys. Chem. B **103**, 10 171 (1999); h) D.G. Hamilton, M. Montalti, L. Prodi, M. Fontani, P. Zanello, J.K.M. Sanders: Chem. Eur. J. **6**, 608 (2000)

22 A. Livoreil, J.-P. Sauvage, N. Armaroli, V. Balzani, L. Flamigni, B. Ventura: J. Am. Chem. Soc. **119**, 12 114 (1997)

23 a) A.C. Benniston, A. Harriman: Angew. Chem. **105**, 1553 (1993); Angew. Chem. Int. Ed. Engl. **32**, 1459 (1993); b) F. Vögtle, W.M. Müller, M. Bauer, K. Rissanen: Angew. Chem. **105**, 1356 (1993); Angew. Chem. Int. Ed. Engl. **32**, 1295 (1993); c) A.C. Benniston, A. Harriman, V.M. Lynch: Tetrahedron Lett. **35**, 1473 (1994); (d) M. Bauer, W.M. Müller, U. Müller, K. Rissanen, F. Vögtle: Liebigs Ann., 649 (1995); e) A.C. Benniston, A. Harriman, V.M. Lynch: J. Am. Chem. Soc. **117**, 5275 (1997); f) N. Armaroli, V. Balzani, J.-P. Collin, P. Gavinã, J.-P. Sauvage, B. Ventura, J. Am. Chem. Soc **121**, 4397 (1999); g) A. Mulder, A. Jukovic, L.N. Lucas, J. van Esch, B.L. Feringa, J. Huskens, D.N. Reinhoudt: Chem. Commun. 2734 (2002)

24 P.R. Ashton, R. Ballardani, V. Balzani, A. Credi, R. Dress, E. Ishow, C.J. Kleverlaan, O. Kocian, J.A. Preece, N. Spencer, J.F. Stoddart, M. Venturi, S. Wenger: Chem. Eur. J. **6**, 3558 (2000)

25 R.C. Ahuja, P.-L. Caruso, D. Möbius, D. Philp, J.A. Preece, H. Ringsdorf, J.F. Stoddart, G. Wildburg: Thin Solid Films **284–285**, 671 (1996)

26 R.C. Ahuja, P.-L. Caruso, D. Möbius, G. Wildburg, H. Ringsdorf, D. Philp, J.A. Preece, J.F. Stoddart: Langmuir **9**, 1534 (1993)

27 C.L. Brown, U. Jonas, J.A. Preece, H. Ringsdorf, M. Seitz, J.F. Stoddart: Langmuir **16**, 1924 (2000)

28 M. Asakawa, M. Higuchi, G. Mattersteig, T. Nakamura, A.R. Pease, F.M. Raymo, T. Shimizu, J.F. Stoddart: Adv. Mater. **12**, 1099 (2000)

29 A.R. Pease, J.O. Jeppesen, J.F. Stoddart, Y. Luo, C.P. Collier, J.R. Heath: Acc. Chem. Res. **34**, 433, (2001)

30 I.C. Lee, C.W. Frank, T. Yamamoto, H.-R. Tseng, A.H. Flood, J.F. Stoddart, J. O Jeppesen: Langmuir **20**, 5809 (2004)

31 H.-R. Tseng, D. Wu, N.X. Fang, X. Zhang, J.F. Stoddart: Chem Phys Chem. **5**, 111 (2004)

32 D.B. Amabilino, M. Asakawa, P.R. Ashton, R. Ballardini, V. Balzani, M. Belohradský, A. Credi, M. Higuchi, F.M. Raymo, T. Shimizu, J.F. Stoddart, M. Venturi, K. Yase: New J. Chem. **22**, 959 (1998)

33 C.P. Collier, J.O. Jeppesen, Y. Luo, J. Perkins, E.W. Wong, J.R. Heath, J.F. Stoddart: J. Am. Chem. Soc. **123**, 12 632 (2001)

34 M.R. Diehl, D.W. Steuerman, H.-R. Tseng, S.A. Vignon, A. Star, P.C. Celestre, J.F. Stoddart, J.R. Heath: Chem Phys Chem. **4**, 1335 (2003)

35 a) C.B. Walsh, E.I. Franses: Thin Solid Films **429**, 71 (2003); b) M. Cecchi, H. Smith, D. Braun: Synth. Met. **121**, 1715 (2001)

36 R. Saf, M. Goriup, T. Steindl, T.E. Hamedinger, D. Sandholzer, G. Hayn: Nature Mater **3**, 323 (2004)

37 M.C. Petty: *Langmuir–Blodgett Films: an introduction* (Cambridge Univ. Press, Cambridge 1996)

38 A. Ulman: *An Introduction to ultrathin organic films* (Academic Press Limited, UK 1991)

39 A. Ulman: Chem. Rev. **95**, 1533 (1996)

40 F. Schreiber: J. Phys.: Condens. Matter **16**, 88 (2004)

41 M. Losche, H.J. Mohwald: Colloid Interface Sci. **131**, 56 (1989)

42 S.-C. Chang, Z. Li, C.N. Lau, B. Larade, R.S. Williams: Appl. Phys. Lett. **83**, 3198 (2003)

43 a) M.S. Dresselhaus, G. Dresselhaus, P. Avouris: *Carbon Nanotubes: Synthesis, Structure Properties and Applications* (Springer-Verlag, Germany 2001); b) P. Avouris, J. Appenzeller, R. Martel, S.J. Wind: Proceedings of the IEEE **91**, 1772 (2003)

44 H. Yu, Y. Luo, K. Beverly, J.F. Stoddart, H.-R. Tseng, J.R. Heath: Angew. Chem. Int. Ed. **42**, 5706 (2003)
45 Y. Chen, D.A.A. Ohlberg, X. Li, D.R. Stewart, R.S. Williams, J.O. Jeppesen, K.A. Nielsen, J.F. Stoddart, D.L. Olynick, E. Anderson: Appl. Phys. Lett. **82**, 1610 (2003)
46 Y. Chen, G.-Y. Jung, D.A.A. Ohlberg, X. Li, D.R. Stewart, J.O. Jeppesen, K.A. Nielsen, J.F. Stoddart, R.S. Williams: Nanotechnology **14**, 462 (2003)
47 D.R. Stewart, D.A.A. Ohlberg, P.A. Beck, Y. Chen, R.S. Williams, J.O. Jeppesen, K.A. Nielsen, J.F. Stoddart: Nano Lett. **4**, 133 (2004)
48 a) J.O. Jeppesen, J. Perkins, J. Becher, J.F. Stoddart: Angew. Chem., Int. Ed. **40**, 1216 (2001); b) J.O. Jeppesen, K.A. Nielsen, J. Perkins, S.A. Vignon, A. Di Fabio, R. Ballardini, J. Becher, J.F. Stoddart: Chem. Eur. J. **9**, 2982 (2003); c) H.-R. Tseng, S.A. Vignon, P.C. Celestre, J. Perkins, A. Di Fabio, R. Ballardini, M.T. Gandolfi, M. Venturi, V. Balzani, J.F. Stoddart: J. F. Chem. Eur. J. **10**, 155 (2004); d) T. Yamamoto, H.-R. Tseng, J.F. Stoddart, V. Balzani, A. Credi, F. Marchioni, M. Venturi: Collect. Czech. Chem. Commun. **68**, 1488 (2003)
49 T.J. Huang, H.-R. Tseng, L. Sha, W. Lu, B. Brough, A.H. Flood, B.-D. Yu, P.C. Celestre, J.P. Chang, J.F. Stoddart, C.-M. Ho: Nano Lett. **4**, 2065 (2004)
50 D.W. Steuerman, H.-R. Tseng, A.J. Peters, A.H. Flood, J.O. Jeppesen, K.A. Nielsen, J.F. Stoddart, J.R. Heath: Angew. Chem., Int. Ed. **43**, 6486 (2004)
51 A.H. Flood, A.J. Peters, S.A. Vignon, D.W. Steuerman, H.-R. Tseng, S. Kang, J.R. Heath, J.F. Stoddart: Chem. Eur. J. **10**, 6558 (2004)
52 a) E.M. Purcell: *Nobel Lectures. Physics 1942–1962* (Elsevier Publishing Company, Amsterdam 1964) p. 219; b) R.R. Ernst: *Nobel Lectures*, *Chemistry 1991–1995* (World Scientific Publishing Co., Singapore 1997) p. 12
53 In fact, the same revolution is underway in single-molecule spectroscopy and microscopy, see: X. Michalet, S. Weiss: C. R. Phys. **3**, 619 (2002)
54 a) J.B. Cui, R. Jordan, M. Burghard, K. Kern: Appl. Phys. Lett. **81**, 3260 (2002); b) A. Nitzan: Ann. Rev. Phys. Chem. **52**, 681 (2001)
55 W.-Q. Deng, R.P. Muller, W.A. Goddard lll: J. Am. Chem. Soc. **126**, 13 562 (2004)
56 Y.H. Jang, S. Hwang, Y.-H. Kim, S.S. Jang, W.A. Goddard lll: J. Am. Chem. Soc. **126**, 12 636 (2004)
57 S.S. Jang, Y.H. Jang, Y.-H. Kim, W. A Goddard lll, A.H. Flood, B.W. Laursen, H.-R. Tseng, J.F. Stoddart, J.O. Jeppesen, J.W. Choi, D.W. Steuerman, E. Delonno, J.R. Heath: J. Am. Chem. Soc. **127**, ASAP (2005)